A new characterization of the North Atlantic eddy-driven jet using 2-dimensional moment analysis

Jacob Perez[1], Amanda C. Maycock[2], Stephen D. Griffiths[3], Steven C. Hardiman[4], and Christine M. McKenna[2]

[1]Centre for Doctoral Training in Fluid Dynamics, University of Leeds, Leeds, UK
[2]School of Earth of Environment, University of Leeds, Leeds, UK
[3]School of Mathematics, University of Leeds, Leeds, UK
[4]Met Office Hadley Centre, Exeter, UK

Correspondence: Jacob Perez (scjp@leeds.ac.uk)

Abstract. We develop a novel technique for characterising the latitude, tilt and intensity of the North Atlantic eddy-driven jet using a feature identification method and two-dimensional moment analysis. Applying this technique to the ERA5 reanalysis, the distribution of daily winter jet latitude is unimodal with a mean of 46°N and a negative skew of -0.07. This is in contrast with the trimodal distribution of the daily Jet Latitude Index (JLI) described by Woollings et al. (2010). We show that our method exhibits less noise than the JLI, casting doubt on the previous interpretations of the trimodal distribution as evidence for regime behaviour of the North Atlantic jet. It also explicitly and straightforwardly handles days where the jet is split. Though climatologically the jet is tilted south-west to north-east, around a fifth of winter days show an opposite tilted jet. Our method is simple, requiring only daily 850 hPa zonal wind data, and diagnoses the jet in a more informative and robust way than previous methods.

1 Introduction

Weather and climate variability in the North Atlantic region is strongly mediated by changes in the position and intensity of the eddy-driven jet (EDJ). Characterising the EDJ across timescales has been the subject of many studies (e.g., Woollings et al., 2010, 2018; Parker et al., 2019; Simpson et al., 2019). While a few techniques have been proposed to diagnose the EDJ position (e.g., Ceppi et al., 2014; Spensberger et al., 2017), the most widely utilised is the Jet Latitude Index (JLI) of Woollings et al. (2010). The JLI is defined as the latitude of the maximum North Atlantic sector-averaged lower-tropospheric zonal wind. In boreal winter, the daily JLI exhibits a trimodal distribution in the North Atlantic (Woollings et al., 2010), which has been interpreted as the jet exhibiting preferred states or regime behaviour. The trimodal behaviour of the JLI has been linked to many phenomena, including storm track variability (Novak et al., 2015), phases of the North Atlantic Oscillation (NAO) (Woollings and Blackburn, 2012), North Atlantic weather regimes (Madonna et al., 2017), state dependent weather predictability (Frame et al., 2011) and stratosphere-troposphere dynamical coupling (Maycock et al., 2020). It is also used as a model evaluation diagnostic (Simpson et al., 2020).

Despite its wide application, the JLI does not provide a full picture of the EDJ and some questions have been raised about the physical interpretation of the trimodal distribution. For example, White et al. (2019) suggested that the northern JLI peak is primarily a result of Greenland tip jets and is not a manifestation of the EDJ. Furthermore, it is unclear how the JLI performs for

25 zonal wind profiles that are bimodal (e.g., Figure 12 of Woollings and Blackburn, 2012). A key feature of the North Atlantic EDJ is its distinct NE-SW tilt due to stationary wave forcing by orography and sea surface temperature patterns (Brayshaw et al., 2009). However, due to zonal averaging over the sector the JLI does not explicitly account for jet tilt. Some studies have proposed methods to calculate the angle of the North Atlantic jet, such as Messori and Caballero (2015) who identify the latitude of the maximum wind speed at each meridian and calculate a Jet Angle Index (JAI) from the line of best fit through

30 the maxima (for a similar approach using the zonal wind see Barriopedro et al., 2022). However, the latitude of the wind speed maximum can show large jumps between meridians, particularly on days when the jet is split and such spurious behaviour needs to be filtered out using arbitrary criteria (Messori and Caballero, 2015; Barriopedro et al., 2022). The method is therefore not straightforward to implement or interpret.

Existing methods for characterising the North Atlantic EDJ therefore have limitations that impact on their reliability and

35 interpretability. The goal of this study is to offer a more robust, yet relatively simple, approach for characterising the North Atlantic EDJ. To achieve this, we apply moment analysis to two-dimensional jet objects identified using a feature-based approach. Moment analysis has been applied to study other geophysical fluid dynamical phenomena, including the Stratospheric Polar Vortex (e.g., Waugh and Randel, 1999; Matthewman et al., 2009) and the nature of coherent vortices in turbulent flows (Mak et al., 2017). This approach has the advantage that it does not rely on spatial averaging and the diagnostics are defined

40 by a collection of points over a specified region of interest rather than a single point. While similar area-weighted definitions of the EDJ position and strength have been used (e.g., Woollings and Blackburn, 2012; Ceppi et al., 2014), they have relied on one-dimensional wind profiles. Using two-dimensional moment analysis we define the position, tilt and the strength of the EDJ in a manner that is simpler and more intelligible than other approaches (e.g., Barriopedro et al., 2022). Another benefit of the method compared to the JLI is that it allows for days where there is no well defined EDJ and can readily accommodate

45 days where the jet is split.

The paper is structured as follows. Section 2 outlines our new methodology for characterising the North Atlantic EDJ. Section 3 compares the new diagnostics with the JLI and JAI. Section 4 relates the new diagnostics to the two leading modes of North Atlantic atmospheric variability, i.e., the North Atlantic Oscillation (NAO) and the East Atlantic Pattern (EA). We finish in Section 5, with conclusions and recommendations.

2 Data and Methods

2.1 Data

We use daily average December-February data from the ERA5 reanalysis dataset over 1979-2020 (Hersbach et al., 2020). All fields are bilinearly interpolated to a regular $2° \times 2°$ grid.

2.2 Identification of EDJ objects

55 EDJ objects are identified using 850 hPa zonal wind (U_{850}) in the same North Atlantic domain ($15°-75°$N, $0°-60°$W) used in the JLI calculation (Woollings et al., 2010). A single wind level is used as there were only minor differences in the results when vertically averaging between 725-950hPa as done in Woollings et al. (2010). Following Woollings et al. (2010), a low-pass Lanczos filter with a 61-day window and a 10 day cut-off frequency is applied to remove short time-scale synoptic features (Duchon, 1979). After applying the filter and accounting for complete winter seasons, this leaves a total of 3701 days in our
60 analysis.

The identification of an Eddy-Driven Jet Object (EDJO) is outlined by the flowchart shown in Figure 1. In detail, each step is as follows:

1. **Locate seed points** - Seed points are identified as local maxima in the U_{850} field, denoted $U_{\max}$. To focus on eddy-driven westerly jets, we define a minimum zonal wind threshold for the seed points, U^*_{850}, which is set to $8\,\mathrm{m\,s^{-1}}$ for this study.
65 This value has been used in other studies to isolate the winter eddy-driven jet (e.g., Woollings et al., 2010). Note that multiple seed points may be identified in an image. If $U_{\max} < U^*_{850}$, then no EDJO is found for that day and the remainder of the steps are skipped.

2. **Flooding** - Starting from the seed point with the largest wind maximum, all neighbouring grid points where $U_{850} \geq U^*_{850}$ are recursively tagged, and a contour enveloping these points is defined as the EDJO (see contour in Figure 1). The
70 neighbouring points include those that are above, below, left, right, and diagonally adjacent to the seed point.

3. **Length check** - A key feature of EDJs is that they are large-scale zonal jets. To remove small scale local wind features we apply two length checks to the EDJO identified in step 2. First, we require the EDJO geodesic length, L, to satisfy $L \geq L^* = 1661$km. To calculate L, a line is extrapolated through the centre of mass of the object (blue circle in Figure 2) and along the major axis (longer black line coming out of the centre of mass in Figure 2), with the distance between
75 the two points that intersect the EDJO edge being used. Definitions of centre of mass and major axis are given in section 2.3. The precise value of L^* is somewhat arbitrary, but we choose it to be the geodesic length of a purely zonal jet at the highest latitude in our domain ($75°$N); note that this is larger than the Rossby radius of deformation in the mid-latitudes of around 1000km.

Second, we require that the EDJO extends over a minimum longitudinal extent, so the longitude range spanned by the
80 EDJO must satisfy $L_\lambda \geq L^*_\lambda = 20°$. If either of these length checks are not met, then the EDJO is rejected.

4. **Remaining Maxima** - To avoid duplicating EDJOs (e.g., if more than 1 maximum lies within a single EDJO), the associated grid points from the previous EDJO are removed from the U_{850} field. If there are any other remaining seed points, then the algorithm returns to step 2 and repeats. This is an advantage over previous methods as it enables the characteristics of split jets to be retained. Once there are no remaining U_{850} maxima, then the algorithm moves to the
85 next time step.

2.3 Moment Diagnostics

Moments are common in statistics to define properties of a distribution, such as the mean or the variance. The definition used here is

$$M_{pq} = \int\int_{\Omega} \lambda^p \phi^q U_{850}(\lambda, \phi) \ r^2 \sin\phi \, d\lambda \, d\phi, \tag{1}$$

where Ω is the EDJO, λ and ϕ are the longitude and latitude, respectively, and $r^2 \sin\phi \, d\lambda \, d\phi$ is the area element on a sphere where r is the radius of the Earth. This formulation is similar to that applied to the potential vorticity distribution for studying the stratospheric polar vortex (e.g., Waugh, 1997). A key difference is that we have chosen to include the strength of the zonal wind as a weighting in the calculation. The inclusion of the weighting factor U_{850} in equation (1) means that our moment calculations (of position and tilt) will reflect regions of stronger zonal wind within the EDJO, which is important in the context of surface impacts. Not incorporating weighting results in purely geometrical moments, as used in some previous studies (e.g., Waugh, 1997; Waugh and Randel, 1999).

The weighting factor also allows us to calculate quantities that are analogues of those used to quantify planar objects in mechanics (mass, centre of mass, major and minor axes), where the weighting factor is simply the surface density (i.e., mass per unit area). We thus define the 'mass' of an EDJO to be $U_{\text{mass}} = M_{00}$, with units of $\text{m}^3\,\text{s}^{-1}$. The average jet strength, U_{mean}, with units of m s^{-1}, is then

$$U_{\text{mean}} = \frac{U_{\text{mass}}}{\int\int_{\Omega} r^2 \sin\phi \, d\lambda \, d\phi}, \tag{2}$$

which is analogous to the average surface density in planar mechanics. Most of the results in this paper represent the largest mass EDJO on a given day, but complete statistics of all EDJO is provided in the supporting information. The jet position can be described by the analogue of the centre of mass, which arises as a longitude $\overline{\lambda}$ and latitude $\overline{\phi}$ defined by

$$\overline{\lambda} = \frac{M_{10}}{M_{00}}, \quad \overline{\phi} = \frac{M_{01}}{M_{00}}. \tag{3}$$

The jet orientation is described by the major axis, which requires analysis of the analogue of the inertia matrix I, here defined by

$$\mathsf{I} = \begin{pmatrix} \tilde{M}_{02} & -\tilde{M}_{11} \\ -\tilde{M}_{11} & \tilde{M}_{20} \end{pmatrix}, \quad \text{where} \quad \tilde{M}_{pq} = \int\int_{\Omega} (\lambda - \overline{\lambda})^p (\phi - \overline{\phi})^q U_{850}(\lambda, \phi) \ r^2 \sin\phi \, d\lambda \, d\phi. \tag{4}$$

The major axis of the EDJO (the longer black line coming from the blue dot in Figure 2a and c) is the direction of the eigenvector associated with the smaller eigenvalue of I. We define the jet tilt, α, to be the angle between the major axis and the line of latitude $\phi = \overline{\phi}$, with positive values indicating a SW-NE tilt, and vice versa. For EDJOs with $\tilde{M}_{20} > \tilde{M}_{02}$, i.e., those elongated longitudinally rather than latitudinally, as should be guaranteed by the length checks in step 3 of section 2.2, there is a simple expression for α:

$$\alpha = \frac{1}{2} \arctan\left(\frac{2\tilde{M}_{11}}{\tilde{M}_{20} - \tilde{M}_{02}}\right), \tag{5}$$

115   as also used in Matthewman et al. (2009).

2.4 JLI and JAI

The JLI is calculated using the method described by Woollings et al. (2010), but applied to the 850 hPa zonal wind field for consistency. Briefly, it is the latitude of the maximum of the North Atlantic sector-averaged U_{850}, where the maximum is found from a 3rd order polynomial to allow for maxima to be found between grid points. The data are time filtered using the same

120   Lanczos filter as above. The jet speed (JLI_{vel}) is the zonal wind at the JLI.

The JAI is calculated as in Messori and Caballero (2015). It uses the daily filtered 850 hPa wind speed ($\mathrm{WS}_{850} = \sqrt{U_{850}^2 + V_{850}^2}$) and locates the maximum at each meridian across the basin. A meridian is ignored when there is a secondary maximum within $4\,\mathrm{m\,s^{-1}}$ of the largest maximum and further than $5°$ in latitude away. This screening is applied to ignore any split jets in the fitting. A linear regression is applied to the maxima across the basin to give a line of best fit. With this the JAI is an angle

125   between $-180°$ and $180°$ that can be calculated from one of the (overlapping) definitions

$$\mathrm{JAI} = \mathrm{atan2}(\Phi_1 - \Phi_0, \Lambda_1 - \Lambda_0) = \begin{cases} \arctan(\frac{\Phi_1 - \Phi_0}{\Lambda_1 - \Lambda_0}) & \text{if } \Lambda_1 - \Lambda_0 > 0, \\ 90° - \arctan(\frac{\Lambda_1 - \Lambda_0}{\Phi_1 - \Phi_0}) & \text{if } \Phi_1 - \Phi_0 > 0, \\ -90° - \arctan(\frac{\Lambda_1 - \Lambda_0}{\Phi_1 - \Phi_0}) & \text{if } \Phi_1 - \Phi_0 < 0, \\ \arctan(\frac{\Phi_1 - \Phi_0}{\Lambda_1 - \Lambda_0}) \pm 180° & \text{if } \Lambda_1 - \Lambda_0 < 0, \\ \text{undefined} & \text{if } \Lambda_1 - \Lambda_0 = 0 \text{ and } \Phi_1 - \Phi_0 = 0, \end{cases} \quad (6)$$

where (Φ_0, Λ_0) and (Φ_1, Λ_1) are the start and end points of the best fit line. Note that this method does not include information on wind direction, only the wind speed. The JLI and JAI methodologies only assign a single jet latitude and tilt for each day, respectively. This is in contrast to our two-dimensional moment diagnostics, which assign values of $(\overline{\lambda}, \overline{\phi})$ and α for each EDJO

130   identified on a given day.

2.5 Large-scale modes of variability

Deseasonalised and standardised daily mean sea level pressure (MSLP) fields are used to calculate the North Atlantic Oscillation (NAO) and the East Atlantic pattern (EA) indices. Following Baker et al. (2018) and McKenna and Maycock (2021), the NAO index is defined as the pressure difference between the gridboxes nearest to Gibraltar ($36°\mathrm{N}, 5.3°\mathrm{W}$) and Iceland

135   ($65°\mathrm{N}, 22.8°\mathrm{W}$). The East Atlantic index is defined as the MSLP anomaly at the gridbox nearest $52°\mathrm{N}, 27.5°\mathrm{W}$ (Moore et al., 2011).

3 Results

3.1 Case study comparisons with JLI and JAI

Figure 2 illustrates two example days (rows) where the moment analysis, JLI and JAI methods are applied. The left column

140 shows U_{850} from which the moment analysis and JLI are calculated, and the right column shows WS_{850} from which JAI is calculated. In the first example day (Figure 2a and 2b), there is close agreement between $\overline{\phi}$ and the JLI (Figure 2a). However, there is strong disagreement between α and the JAI, which show opposite signs (Figure 2b). This is because the JAI calculation does not account for wind direction and erroneously connects points with intense westerly and easterly zonal wind (Figure 2a), leading to a positive JAI that does not characterise the tilt of the westerly jet on this day. Furthermore, the meridians are

145 only sparsely sampled because of the JAI criterion to disregard split jets. Therefore, the JAI calculation can result in inaccurate assessments of tilt for several reasons.

In the second example (Figure 2c and d), the JAI and α are in close agreement showing a highly tilted jet structure (Figure 2d). However, there is a marked difference between the JLI and $\overline{\phi}$ on this day (Figure 2c). This discrepancy is attributable to the specific EDJ structure comprising a highly tilted jet with an intensified equatorward flank. As a result of the stronger equa-

150 torward westerlies, the JLI shows a southerly position. In contrast, $\overline{\phi}$ exhibits a more central latitude that better encapsulates the overall jet structure on this day. These two examples illustrate that the JLI and JAI can provide misleading results, and that the moment-based analysis has the potential to overcome some of their respective limitations.

We now consider temporal variability of the different EDJ diagnostics. Over a single winter, the JLI can display large changes in a short period (Woollings et al., 2010; Madonna et al., 2017). These changes have been interpreted as regime shifts, with

155 sudden transitions between "preferred" jet latitudes (Hannachi et al., 2011; Franzke et al., 2011; Novak et al., 2015). Figure 3 shows the evolution of the JLI and $\overline{\phi}$ for the winter of 2016/17. During some periods, the JLI and $\overline{\phi}$ show similar jet positions. However, at other times the JLI displays rapid and large changes that are not consistently mirrored in $\overline{\phi}$. Figure 3 also shows that at certain times the moment based method identifies a split jet (pink markers) that implicitly cannot be captured by the JLI algorithm. Overall, $\overline{\phi}$ exhibits a more smoothly varying temporal behaviour within the season.

160 To examine what is occurring during some of the periods in 2016/17 where the two measures of jet latitude show different behaviours, we select three snapshots from the winter (black arrows in Figure 3) and plot the U_{850} maps for these consecutive days (Figure 4). The 10th and 11th December 2016 coincide with an $8°$ decrease in JLI but little change in $\overline{\phi}$. Figures 4a and 4b reveal a broad EDJ in this period. When the EDJ is broad, the JLI is very sensitive to relatively small fluctuations in the zonal wind field within the EDJO. However, $\overline{\phi}$ is less sensitive to the local fluctuations and varies relatively little between these

165 days, which better captures that the overall EDJO is largely unchanged.

In early January 2017, an atmospheric blocking event in the North Atlantic results in a split EDJ. During this period, the JLI shows a northerly jet, but this does not well characterise the overall circulation pattern (Figures 4c and 4d). In contrast, the moment-based method locates two separate EDJOs which better reflects the split jet structure.

Between 22nd to 23rd January 2017, the JLI shows a large north-to-south transition of around $25°$ in a single day, while $\overline{\phi}$

170 shows almost no change in latitude. Figures 4e and 4f show the jet is highly tilted in this period. Initially, the JLI locates the

maximum wind at a northern latitude near the tip of Greenland. Subsequently, a very modest strengthening in the westerlies over West Africa causes a large equatorward shift in the JLI the following day. Remarkably, the large-scale U_{850} field remains relatively unaltered during this 'transition', and this is reflected not only in $\overline{\phi}$ but also in the value of α in its respective time series (not shown).

175   These three examples illustrate the limitations of JLI as a measure of the jet. We conclude that JLI may provide misleading results in the following cases: 1) a broad jet, 2) a highly tilted jet, 3) a split jet, and 4) when there is no well defined EDJ. In all these cases, our moment based method offers a more detailed and informative picture of the overall jet structure. To further illustrate this, Figure 5 shows timeseries of the frequency of large shifts in jet latitude based on JLI and $\overline{\phi}$. A large shift is defined as a change in latitude $\geq 10°$ between consecutive days. For $\overline{\phi}$ this is calculated only on the days where a single EDJO

180 is defined, to reduce potential switching between the largest mass object on consecutive days with two EDJOs. As shown above, days with a single EDJO are less sensitive to broad or tilted jet cases. The mean winter frequency of large shifts in the JLI is 7 times larger than for $\overline{\phi}$. This indicates that the feature of the JLI exhibiting a sudden shift, which was highlighted in the example winter in Figure 4, is generally representative of other years.

3.2   Winter statistics

185 The analysis over all selected years finds 1.7% of days without an EDJO, 93.5% of days with one EDJO and 4.8% of days with two EDJOs. Unless otherwise stated, the results shown here are characteristics based on the largest mass object on any given day. The locations of the centres of mass of EDJOs are shown in Figure 6. The spatial distribution of all centres of mass (Figure 6a) shows a trimodal structure, with a high concentration of points at the basin's center and two smaller density maxima situated towards the northeast and southwest quadrants of the basin. These outlier regions coincide with the majority

190 of the locations of two EDJO days (blue points) indicating sites where split jets occur. The distribution of centres of mass for the largest mass EDJO on each day (Figure 6b) is largely similar to Figure 6a, except that the north-east secondary maximum decreases indicating these EDJOs are generally lower in mass than the south-west located EDJOs on split jet days. This is consistent with the smaller area of the high latitude EDJOs.

    The distributions of $\overline{\phi}$ and JLI on all days are shown in Figures 7a and 7b. Equivalent distributions for all EDJOs are shown

195 in Supplementary Information Figure S1. The two measures show comparable ranges of values but different structures. Note that $\overline{\phi}$ has a (roughly Gaussian) unimodal distribution, with mean $\mu(\overline{\phi}) = 45.7°$. There is a negative skew, which is particularly evident on the equatorward flank, at about $37°$. As noted in many previous studies, JLI shows a trimodal distribution with maxima near 37°N, 45°N and 57°N. The distribution of differences between $\overline{\phi}$ and JLI binned by JLI value (Figure 7c) reveals that when JLI is in the southern mode (JLI $< 40°$; 12.1% of days), $\overline{\phi}$ tends to take more poleward values than the JLI with a

200 median difference of $0.74°$ (and standard deviation $\sigma = 3.7°$). When the JLI is located in the northern mode (JLI $> 52°$; 37.4% of days), $\overline{\phi}$ tends to be more equatorward than the JLI with a median value of $5.2°$ ($\sigma = 7.23°$). When JLI is located in the central mode ($40° \leq$ JLI $\leq 52°$; 48.5% of days), the two methods show the highest agreement with a median difference of $-1.0°$ and a standard deviation of $2.28°$. Therefore the fundamental differences in the shape of the distributions predominantly arise from

days where the JLI is in the northern or southern modes. The distribution of $\overline{\phi}$ including all EDJOs, and not just the largest
205   mass one, is very similar and also does not show multi-modal structure (Supplementary Figure S1a).

    It was previously shown in Section 3.1 that strongly tilted jets can lead to disparities between $\overline{\phi}$ and JLI. To further investigate
this, Figure 8 shows composites of U_{850} binned by α where $\alpha \geq 0$, with the values of $\overline{\phi}$ and JLI overplotted as calculated
from the (single) composite field of U_{850}. As α increases, the difference between the JLI and $\overline{\phi}$ also increases, with the JLI
identifying progressively more northerly values than $\overline{\phi}$ on average. The composite U_{850} field for $\alpha \geq 30°$ (Figure 8c) shows
210   two wind maxima near 30°N, 60°W and 62°N, 10°W, which suggests an influence from split jet days when α is strongly
positive and also potentially Greenland tip jet days (White et al., 2019). This shows that the substantial differences between $\overline{\phi}$
and the JLI when JLI$\geq$52°N (Figure 7c) are linked to highly tilted jets, similar to the case shown in Figure 4c. This is further
evidenced in Figure 9 which shows the daily $\overline{\phi}$ minus JLI differences plotted against α (panel a) and U_{mean} (panel b). On
average, the differences between $\overline{\phi}$ and JLI are largest when the jet is weaker and more tilted.

215   The distributions of α and JAI in Figures 7d and 7e show a mean positive tilt for both measures ($\mu(\alpha)$=7.9°, $\mu(\mathrm{JAI}) = 11.7°$),
consistent with the winter U_{850} climatology. The JAI exhibits higher variability than α with $\sigma = 15.7°$, while α has a value of
11.7°. The median α-JAI difference is -3.6° when JAI$\geq$0 and 10.9° when JAI$<$0, indicating that JAI tends to produce larger
magnitudes of tilt than α (Figure 7f). The α-JAI differences also show a large spread, with σ=13.4° for JAI$\geq$0 and σ=13.7°
for JAI$<$0, indicating many outlier days where the two measures of tilt are substantially different. Some of these days are
220   associated with opposite signs of α and JAI owing to the fact that JAI uses wind speed without accounting for wind direction.

    The case study winter shown in Figure 3 showed weaker time variability in $\overline{\phi}$ than JLI. We now examine the overall per-
sistence of the jet diagnostics. The autocorrelation function (ACF) for each of the JLI and $\overline{\phi}$ is shown in Figure 10a. There
is a systematically higher ACF of $\overline{\phi}$ for lags of up to 10 days, which is consistent with the emerging picture of a more noisy
behaviour in JLI which would tend to reduce the ACF. The ACFs for α and JAI are similar. Interestingly, JLI$_{\mathrm{vel}}$ has a higher
225   ACF than both U_{mean} and U_{max}, which is the closest measure to JLI$_{\mathrm{vel}}$. The lower ACF in U_{max} may be being caused by the
search over the two-dimensional field, which may inherently cause some noise. The lower ACF in U_{mean} is surprising as it
is a mean over the EDJO, whereas JLI$_{\mathrm{vel}}$ is the maximum at a single point. It is possible that the sectoral averaging may be
smoothing some of the noise in speed and hence resulting in a higher ACF in JLI$_{\mathrm{vel}}$. The highest ACF for the strength comes
from U_{mass} which is interesting, as U_{mass} and U_{mean} are related simply by the area of the EDJO (see equation (2)).

230   **3.3   Relationship between moment jet metrics**

    We now investigate the cross-relationships between some of the jet parameters. Figure 11 displays scatterplots illustrating
the relationships between $\overline{\phi}$, α, and U_{mean}. There is little to no correlation between $\overline{\phi}$ and both α and U_{mean}, with a Pearson
correlation coefficient of 0.1 in each case (Figure 11a and 11b). However, in Figure 11c, a noticeable cone-shaped relationship
between U_{mean} and α is observed, indicating that a stronger North Atlantic EDJ tends to be more zonal. Referring back to Figure
235   11b, the strongest zonal jets are situated close to the mean of $\overline{\phi}$. As the tilt increases while moving poleward, the jet strength
tends to decrease. This behaviour aligns with previous studies that have investigated the relationship between jet latitude and
strength (Woollings et al., 2018).

4 Relationship to large-scale modes of variability

The North Atlantic Oscillation (NAO) and the East Atlantic pattern (EA) are the two leading modes of atmospheric variability
240 in the North Atlantic sector. While these modes do not explain the full spectrum of EDJ variability, they are associated with substantial variations in jet latitude and strength (Woollings et al., 2010).

Figure 12 shows scatterplots of the daily NAO and EA indices coloured by $\overline{\phi}$ (Figure 12a), the JLI (Figure 12b), U_{mean} (Figure 12c), JLI_{vel} (Figure 12d), α (Figure 12e) and JAI (Figure 12f). The mean μ and standard deviation σ for each quadrant are given in brackets. Figure 12b reproduces the finding of Woollings et al. (2010) that jet latitude increases moving clockwise around
245 the phase space, with a discontinuity between the highest and lowest JLI values occurring within the NAO-/EA- quadrant. The equivalent plot for $\overline{\phi}$ shows similar behaviour but the variance within each quadrant is smaller, resulting in a more smoothly varying distribution. The discontinuity in the NAO-/EA- quadrant is associated with European/Scandinavian blocking and weak jets, where the jet either diverts to the north or south around the block (see Figure 4a in Madonna et al., 2017). Days with zero and two EDJOs only lie within the NAO-/EA- part of the phase space (shown in the Supplementary Figure S2).
250 The patterns of U_{mean} and JLI_{vel} in the NAO/EA phase space are very similar, though the range of values is smaller for U_{mean}. The strongest jets span the outer envelope of the distribution across the largest EA+ and NAO+ points. Conversely the weakest jets are confined to NAO-/EA- which often coincide with blocking. The values of JAI and α show a more isotropic distribution within the phase space, but there is substantially larger variability in JAI than in α, as shown in Figure 7. For α, generally the stronger NAO- states coincide with more negatively tilted EDJs, whereas NAO+ is associated with positive tilt.

5 Discussion and Conclusions

The Jet Latitude Index (JLI) of Woollings et al. (2010) is commonly employed to characterise the location of the North Atlantic Eddy-Driven Jet (EDJ) (e.g., Woollings et al., 2018; Simpson et al., 2020; Maycock et al., 2020). The JLI shows a trimodal distribution of daily North Atlantic winter values, which has become a benchmark for theoretical and numerical models alike. A separate method, the Jet Angle Index (JAI) of Messori and Caballero (2015), has been proposed to diagnose the jet tilt based
260 on lower tropospheric wind speed. Both of these methods have limitations, in part due to the use of zonal averaging for the JLI and the use of wind speed, but not direction, for the JAI. To address these limitations, we have developed an intuitive and simple method that extracts Eddy-Driven Jet Objects (EDJOs) within the North Atlantic basin from a U_{850} field. By calculating two-dimensional moments of the EDJO, we define the position of the EDJ using the an analogue of the centre of mass $(\overline{\phi}, \overline{\lambda})$, its strength ($U_{\text{mean}}$) and tilt ($\alpha$). The same approach can also be used to extract information on jet width.
265 Our study has several key results:

1. Our jet identification method more robustly characterises the jet structure on days where the jet is broad, highly tilted, split or not well defined, as compared to the JLI.

2. The time variability of $\overline{\phi}$ shows fewer large amplitude 'jumps' between consecutive days as compared to JLI. Examination of cases suggests these jumps in JLI can be spurious resulting from selecting one of several competing single

270   maximum and do not reflect meaningful changes in the jet structure. The autocorrelation function of $\overline{\phi}$ shows greater persistence than JLI between days 2-9.

3. The statistics of $\overline{\phi}$ over all winter days do not show a trimodal distribution as seen for the JLI. The distribution has a mean of 45.7° and a skewness of -0.07. The daily differences between $\overline{\phi}$ and the JLI tend to be larger for wider jets and highly tilted jets. When compositing low level zonal wind for the same range of values, the two measures pick out
275   similar patterns of large-scale circulation.

4. The distribution of jet tilt α is more Gaussian with a mean of 7.9°. Around 20% of days show a negative tilt.

The results presented here suggest previous studies analysing time variability of the JLI and its connection to dynamical processes should be revisited (e.g., Novak et al., 2015; Franzke et al., 2011). Furthermore, past work to connect the JLI trimodal structure to weather types or weather regimes should be revisited in light of the unimodal structure of $\overline{\phi}$ (Madonna
280   et al., 2017). Future work will examine the impact of teleconnections on the North Atlantic jet, such as from El Niño Southern Oscillation (Hardiman et al., 2019; Ineson and Scaife, 2008) and the Indian Ocean Dipole (Hardiman et al., 2020), as well as the jet response to external forcings. Future work will also consider the application of the method to the summer North Atlantic circulation.

Barriopedro et al. (2022) recently proposed a new multi-parametric method to characterise the structure of the North Atlantic
285   jet in more detail. However, most of the measures they consider can be derived from the moment analysis applied here and their method is considerably more complicated to implement. The method presented here is simple to implement, requiring only 850 hPa zonal wind fields, and has only three tuneable parameters. We encourage the community to adopt this as a new approach to characterising the North Atlantic EDJ.

References

Baker, L. H., Shaffrey, L. C., Sutton, R. T., Weisheimer, A., and Scaife, A. A.: An Intercomparison of Skill and Overconfidence/Undercon-
300   fidence of the Wintertime North Atlantic Oscillation in Multimodel Seasonal Forecasts, Geophysical Research Letters, 45, 7808–7817,
       https://doi.org/https://doi.org/10.1029/2018GL078838, 2018.

Barriopedro, D., Ayarzagüena, B., García-Burgos, M., and García-Herrera, R.: A multi-parametric perspective of the North Atlantic eddy-
       driven jet, Climate Dynamics, https://doi.org/10.1007/s00382-022-06574-w, 2022.

Brayshaw, D. J., Hoskins, B., and Blackburn, M.: The Basic Ingredients of the North Atlantic Storm Track. Part I: Land–Sea Contrast and
305   Orography, Journal of the Atmospheric Sciences, 66, 2539–2558, https://doi.org/10.1175/2009jas3078.1, 2009.

Ceppi, P., Zelinka, M. D., and Hartmann, D. L.: The response of the Southern Hemispheric eddy-driven jet to future changes in shortwave
       radiation in CMIP5, Geophysical Research Letters, 41, 3244–3250, https://doi.org/10.1002/2014GL060043, 2014.

Duchon, C. E.: Lanczos Filtering in One and Two Dimensions, Journal of Applied Meteorology and Climatology,
       https://doi.org/10.1175/1520-0450(1979)018<1016:lfioat>2.0.co;2, 1979.

310 Frame, T. H. A., Ambaum, M. H. P., Gray, S. L., and Methven, J.: Ensemble prediction of transitions of the North Atlantic eddy-driven jet,
       Quarterly Journal of the Royal Meteorological Society, 137, 1288–1297, https://doi.org/https://doi.org/10.1002/qj.829, 2011.

Franzke, C., Woollings, T., and Martius, O.: Persistent Circulation Regimes and Preferred Regime Transitions in the North Atlantic, Journal
       of the Atmospheric Sciences, 68, 2809–2825, https://doi.org/10.1175/jas-d-11-046.1, 2011.

Hannachi, A., Woollings, T., and Fraedrich, K.: The North Atlantic jet stream: a look at preferred positions, paths and transitions, Quarterly
315   Journal of the Royal Meteorological Society, 138, 862–877, https://doi.org/10.1002/qj.959, 2011.

Hardiman, S. C., Dunstone, N. J., Scaife, A. A., Smith, D. M., Ineson, S., Lim, J., and Fereday, D.: The Impact of Strong El Niño and La
       Niña Events on the North Atlantic, Geophysical Research Letters, 46, 2874–2883, https://doi.org/10.1029/2018GL081776, 2019.

Hardiman, S. C., Dunstone, N. J., Scaife, A. A., Smith, D. M., Knight, J. R., Davies, P., Claus, M., and Greatbatch, R. J.: Predictability of
       European winter 2019/20: Indian Ocean dipole impacts on the NAO, Atmospheric Science Letters, 21, https://doi.org/10.1002/asl.1005,
320   2020.

Hersbach, H., Bell, B., Berrisford, P., Hirahara, S., Horányi, A., Muñoz-Sabater, J., Nicolas, J., Peubey, C., Radu, R., Schepers, D., Sim-
       mons, A., Soci, C., Abdalla, S., Abellan, X., Balsamo, G., Bechtold, P., Biavati, G., Bidlot, J., Bonavita, M., De Chiara, G., Dahlgren,
       P., Dee, D., Diamantakis, M., Dragani, R., Flemming, J., Forbes, R., Fuentes, M., Geer, A., Haimberger, L., Healy, S., Hogan, R. J.,
       Hólm, E., Janisková, M., Keeley, S., Laloyaux, P., Lopez, P., Lupu, C., Radnoti, G., de Rosnay, P., Rozum, I., Vamborg, F., Vil-
325   laume, S., and Thépaut, J.-N.: The ERA5 global reanalysis, Quarterly Journal of the Royal Meteorological Society, 146, 1999–2049,
       https://doi.org/https://doi.org/10.1002/qj.3803, 2020.

Ineson, S. and Scaife, A. A.: The role of the stratosphere in the European climate response to El Niño, Nature Geoscience 2009 2:1, 2, 32–36,
       https://doi.org/10.1038/ngeo381, 2008.

Madonna, E., Li, C., Grams, C. M., and Woollings, T.: The link between eddy-driven jet variability and weather regimes in the North
330   Atlantic-European sector, Quarterly Journal of the Royal Meteorological Society, 143, 2960–2972, https://doi.org/10.1002/qj.3155, 2017.

Mak, J., Griffiths, S. D., and Hughes, D. W.: Vortex disruption by magnetohydrodynamic feedback, Physical Review Fluids, 2,
       https://doi.org/10.1103/physrevfluids.2.113701, 2017.

Matthewman, N. J., Esler, J. G., Charlton-Perez, A. J., and Polvani, L. M.: A New Look at Stratospheric Sudden Warmings. Part III: Polar
       Vortex Evolution and Vertical Structure, Journal of Climate, 22, 1566–1585, https://doi.org/10.1175/2008jcli2365.1, 2009.

335 Maycock, A. C., Masukwedza, G. I. T., Hitchcock, P., and Simpson, I. R.: A Regime Perspective on the North Atlantic Eddy-Driven Jet
        Response to Sudden Stratospheric Warmings, Journal of Climate, 33, 3901–3917, https://doi.org/10.1175/jcli-d-19-0702.1, 2020.

    McKenna, C. M. and Maycock, A. C.: Sources of Uncertainty in Multimodel Large Ensemble Projections of the Winter North Atlantic
        Oscillation, Geophysical Research Letters, 48, e2021GL093 258, https://doi.org/https://doi.org/10.1029/2021GL093258, e2021GL093258
        2021GL093258, 2021.

340 Messori, G. and Caballero, R.: On double Rossby wave breaking in the North Atlantic, Journal of Geophysical Research: Atmospheres, 120,
        11,129–11,150, https://doi.org/https://doi.org/10.1002/2015JD023854, 2015.

    Moore, G. W. K., Pickart, R. S., and Renfrew, I. A.: Complexities in the climate of the subpolar North Atlantic: a case study from the winter
        of 2007, Quarterly Journal of the Royal Meteorological Society, 137, 757–767, https://doi.org/10.1002/qj.778, 2011.

    Novak, L., Ambaum, M. H. P., and Tailleux, R.: The Life Cycle of the North Atlantic Storm Track, Journal of the Atmospheric Sciences, 72,
345   821 – 833, https://doi.org/10.1175/JAS-D-14-0082.1, 2015.

    Parker, T., Woollings, T., Weisheimer, A., O'Reilly, C., Baker, L., and Shaffrey, L.: Seasonal Predictability of the Winter North Atlantic
        Oscillation From a Jet Stream Perspective, Geophysical Research Letters, 46, 10 159–10 167, https://doi.org/10.1029/2019gl084402, 2019.

    Simpson, I. R., Yeager, S. G., McKinnon, K. A., and Deser, C.: Decadal predictability of late winter precipitation in western Europe through
        an ocean–jet stream connection, Nature Geoscience, 12, 613–619, https://doi.org/10.1038/s41561-019-0391-x, 2019.

350 Simpson, I. R., Bacmeister, J., Neale, R. B., Hannay, C., Gettelman, A., Garcia, R. R., Lauritzen, P. H., Marsh, D. R., Mills, M. J., Medeiros,
        B., and Richter, J. H.: An Evaluation of the Large-Scale Atmospheric Circulation and Its Variability in CESM2 and Other CMIP Models,
        Journal of Geophysical Research: Atmospheres, 125, https://doi.org/10.1029/2020jd032835, 2020.

    Spensberger, C., Spengler, T., and Li, C.: Upper-Tropospheric Jet Axis Detection and Application to the Boreal Winter 2013/14, Monthly
        Weather Review, 145, 2363–2374, https://doi.org/10.1175/mwr-d-16-0467.1, 2017.

355 Waugh, D. N. W.: Elliptical diagnostics of stratospheric polar vortices, Quarterly Journal of the Royal Meteorological Society, 123,
        1725–1748, https://doi.org/10.1002/qj.49712354213, 1997.

    Waugh, D. W. and Randel, W. J.: Climatology of Arctic and Antarctic Polar Vortices Using Elliptical Diagnostics, Journal of the Atmospheric
        Sciences, 56, 1594–1613, https://doi.org/10.1175/1520-0469(1999)056<1594:coaaap>2.0.co;2, 1999.

    White, R. H., Hilgenbrink, C., and Sheshadri, A.: The Importance of Greenland in Setting the Northern Preferred Position of the North
360   Atlantic Eddy-Driven Jet, Geophysical Research Letters, 46, 14 126–14 134, https://doi.org/10.1029/2019gl084780, 2019.

    Woollings, T. and Blackburn, M.: The North Atlantic Jet Stream under Climate Change and Its Relation to the NAO and EA Patterns, Journal
        of Climate, 25, 886–902, https://doi.org/10.1175/jcli-d-11-00087.1, 2012.

    Woollings, T., Hannachi, A., and Hoskins, B.: Variability of the North Atlantic eddy-driven jet stream, Quarterly Journal of the Royal
        Meteorological Society, https://doi.org/10.1002/qj.625, 2010.

365 Woollings, T., Barnes, E., Hoskins, B., Kwon, Y.-O., Lee, R. W., Li, C., Madonna, E., McGraw, M., Parker, T., Rodrigues, R., Spensberger,
        C., and Williams, K.: Daily to Decadal Modulation of Jet Variability, Journal of Climate, 31, 1297–1314, https://doi.org/10.1175/jcli-d-
        17-0286.1, 2018.
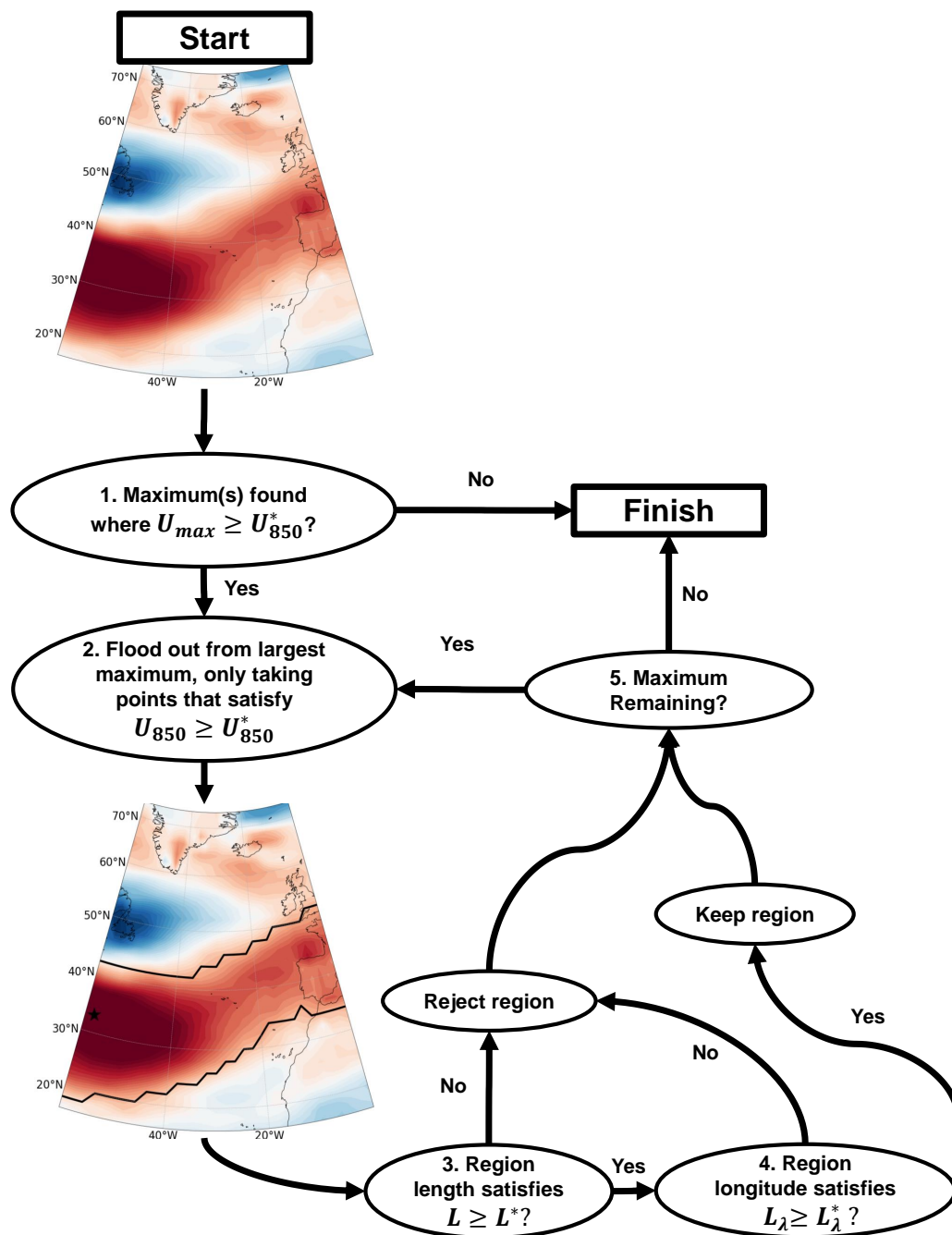
Figure 1. Algorithm for identification of Eddy-Driven Jet Objects (EDJOs). In the map, the black star is the seed point and the black contour is the EDJO found from the seed point.
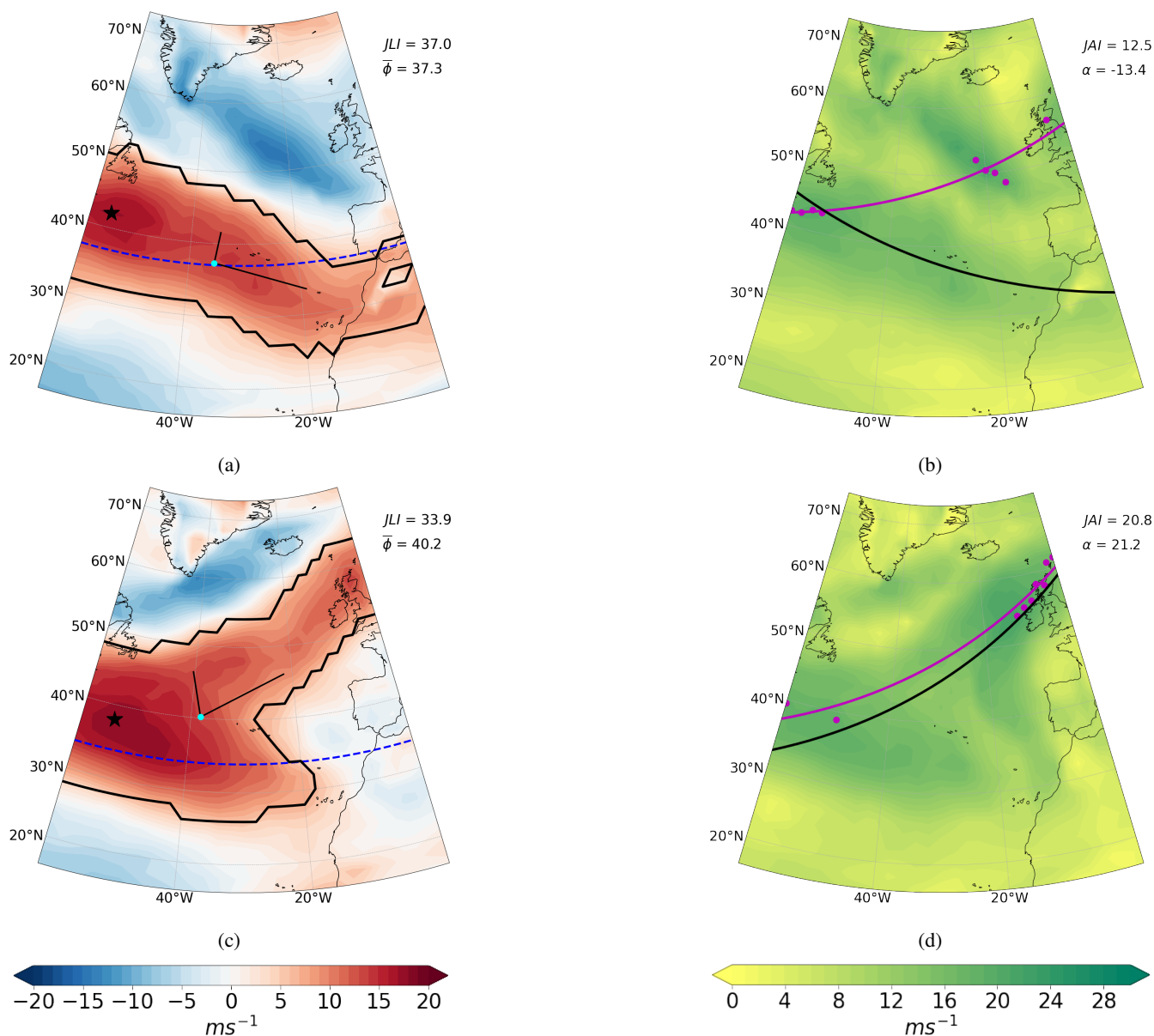
Figure 2. U_{850} (left) and wind speed (right) for two different days (rows). The dashed line denotes the JLI. The black star denotes the location of the seed point and the light blue dot is the position of $(\overline{\lambda}, \overline{\phi})$ the centre of mass. In (b) and (d), the magenta circles are the maxima at each meridian and the magenta line is the result of linear regression fitted to those maxima following Messori and Caballero (2015). The JAI in (b) and (d) is calculated from the end points of the magenta line and the solid black line is the tilt given by α which comes from the black lines coming from the centre of mass in (a) and (c). Values of the indices for the respective methods are given in the top right of each panel.
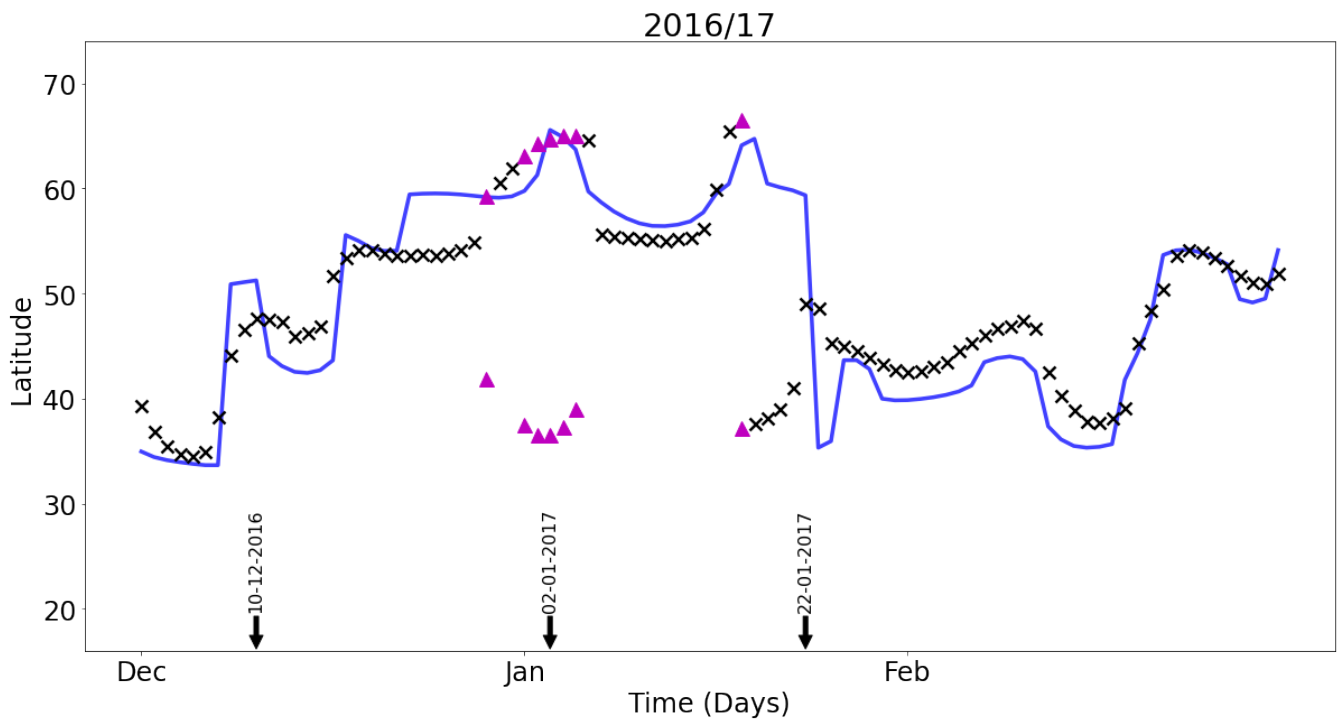
Figure 3. Time series of $\overline{\phi}$ (black crosses) and the JLI (blue line) for the boreal winter 2016/17. Pink triangles represent days with two EDJOs. The black arrows indicate the starting date for the consecutive day cases shown in Figure 4.
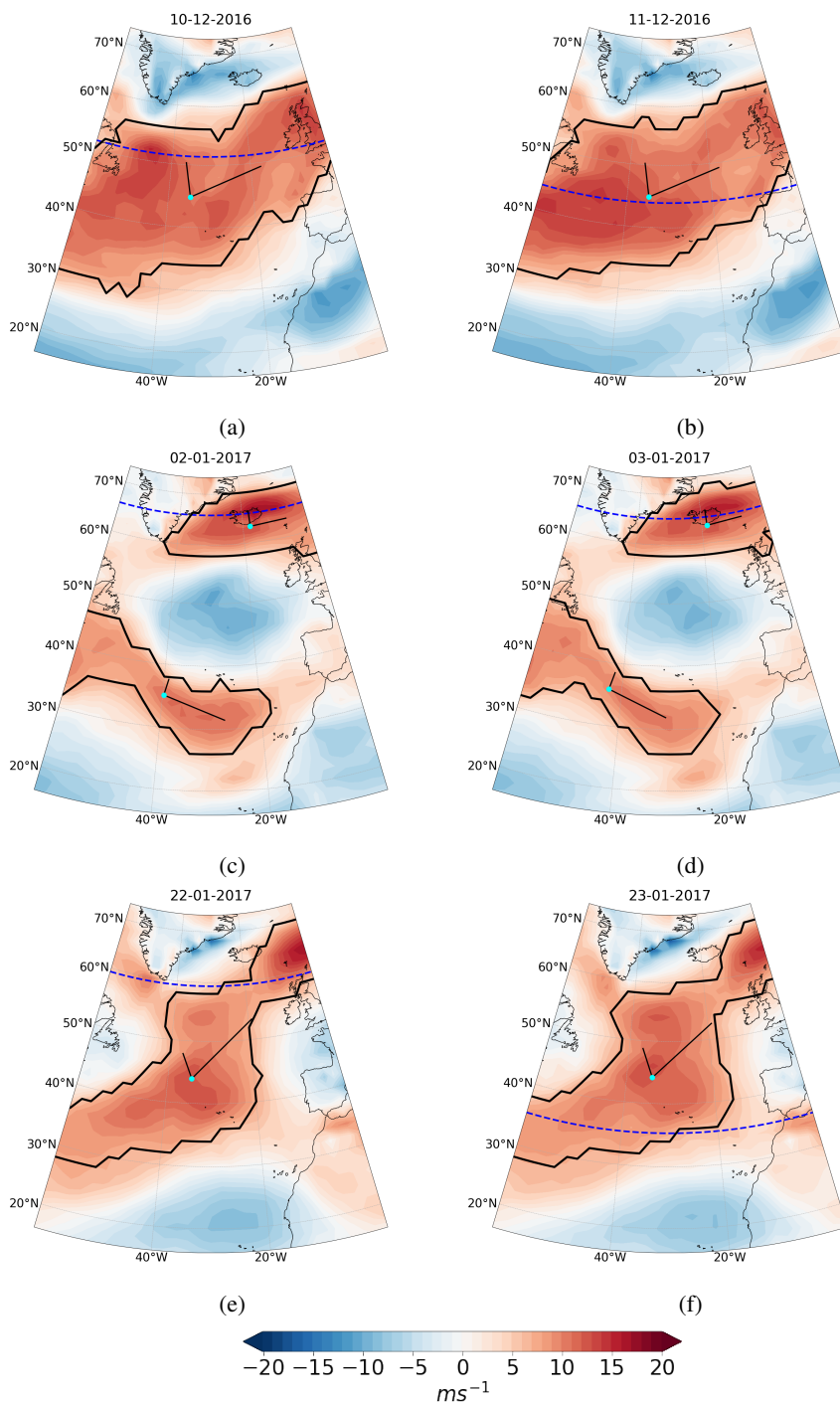
Figure 4. U_{850} for example days in winter 2016/17 taken from Figure 3. Dashed dark blue lines denotes JLI value on each day. Solid contour(s) denote EDJO(s). Light blue dots denote the centre of mass $(\overline{\lambda}, \overline{\phi})$ of the EDJO with the longer black line defining the major axis and the shorter the minor axis.
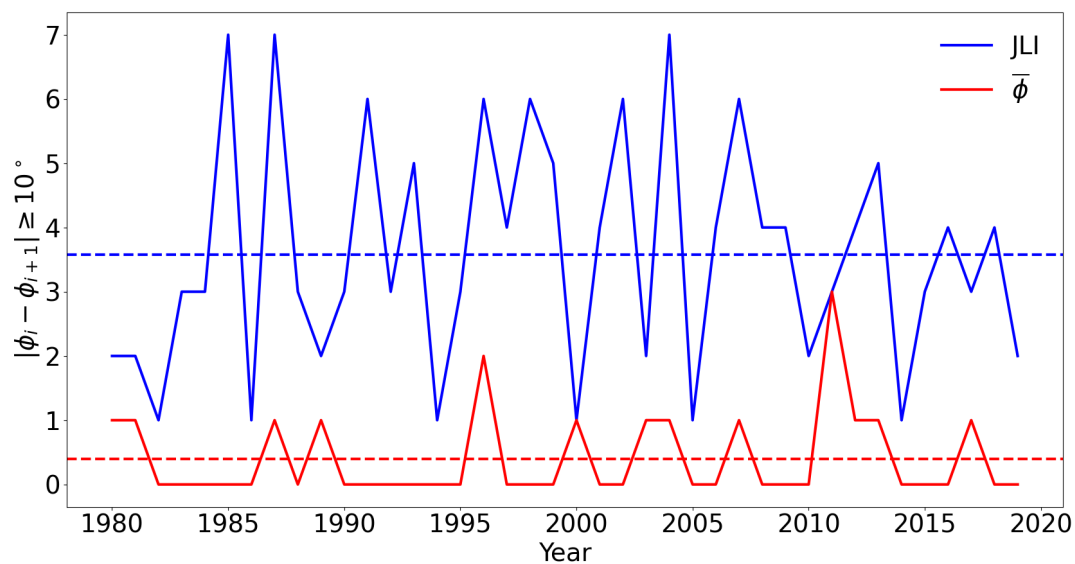
Figure 5. Frequency per winter of large shifts ($\geq 10°$) in jet latitude between consecutive days. Blue shows JLI shifts and red shows $\overline{\phi}$ shifts. The dashed lines show the average frequency per winter over the entire period. Calculations only account for days with one EDJO.

(a)

(b)
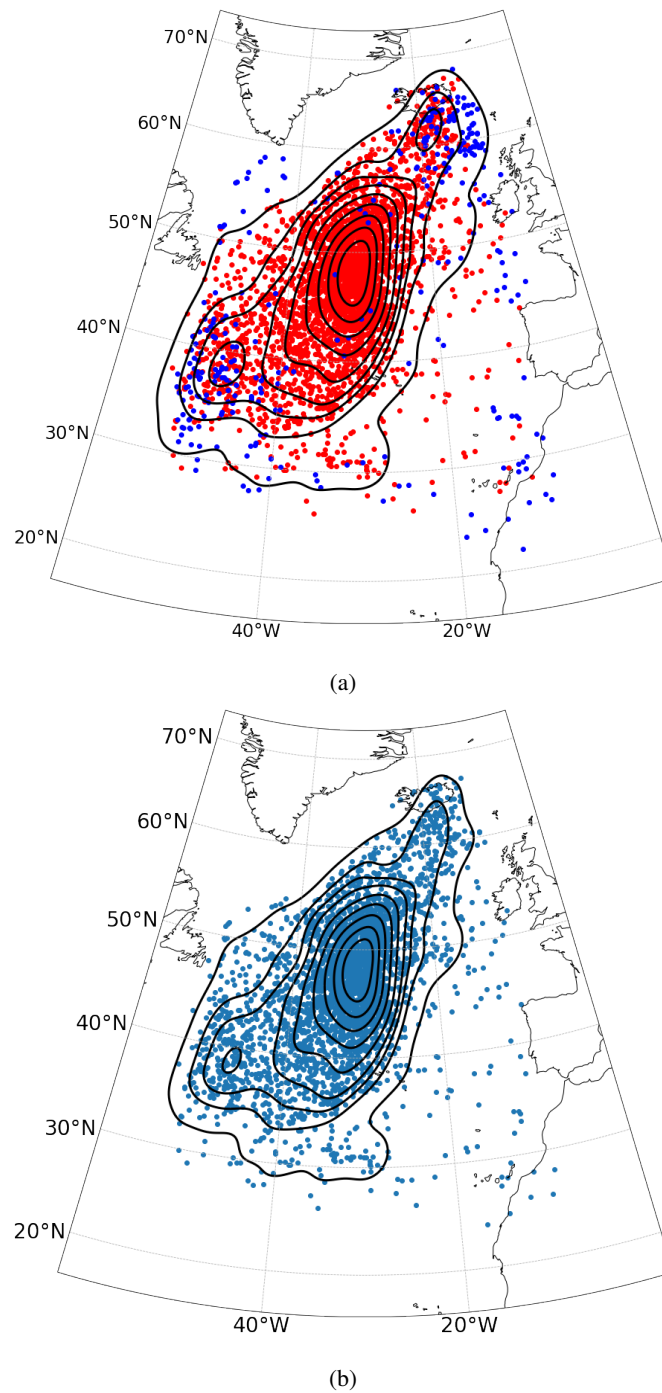
Figure 6. Distributions of EDJO centre of masses $(\overline{\lambda}, \overline{\phi})$ for (a) all EDJOs and (b) the largest U_{mass} EDJO on each day. Colours in (a) represent whether one (red) or two (blue) EDJOs are identified on a given day. Black contours show a two-dimensional KDE of the distribution.
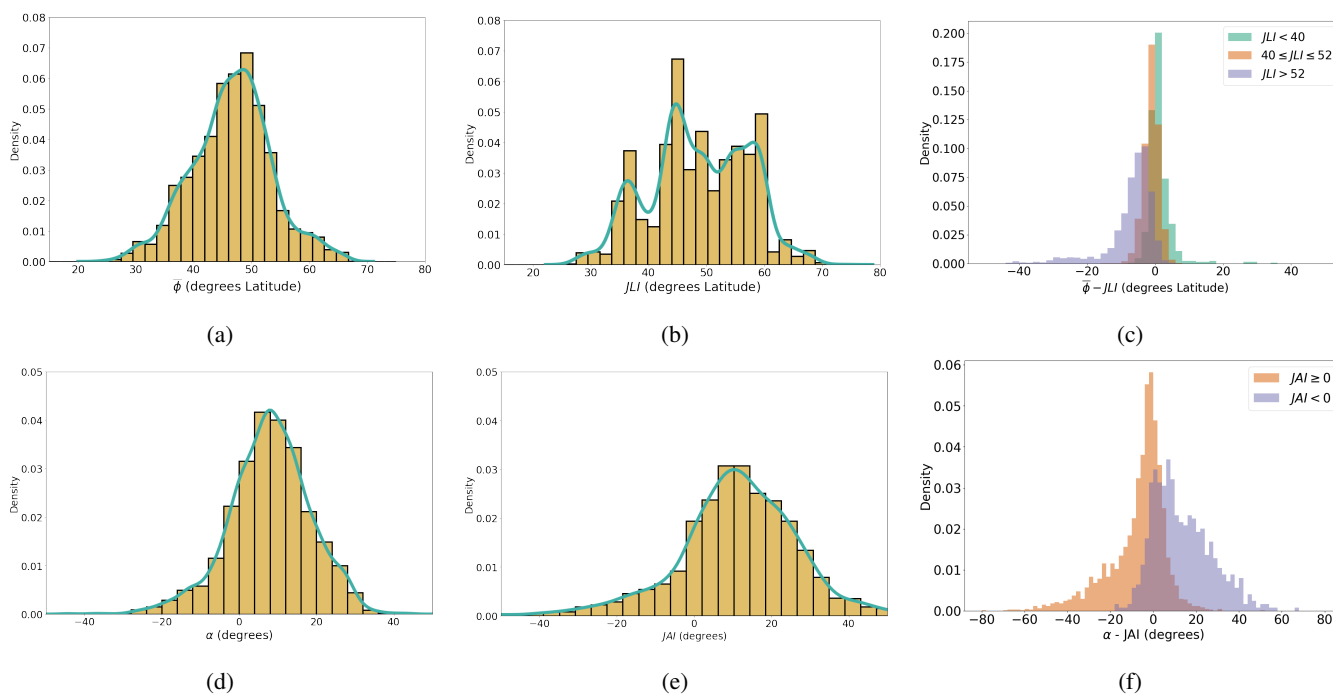
Figure 7. Distributions of all winter daily (a) $\overline{\phi}$, (b) JLI, (c) $\overline{\phi} - JLI$, (d) α, (e) JAI and (f) $\alpha - JAI$. In (c) $\overline{\phi} - JLI$ is coloured according to the three JLI modes and in (f) $\alpha - JAI$ is coloured based on the sign of JAI. Bin size is $2°$.
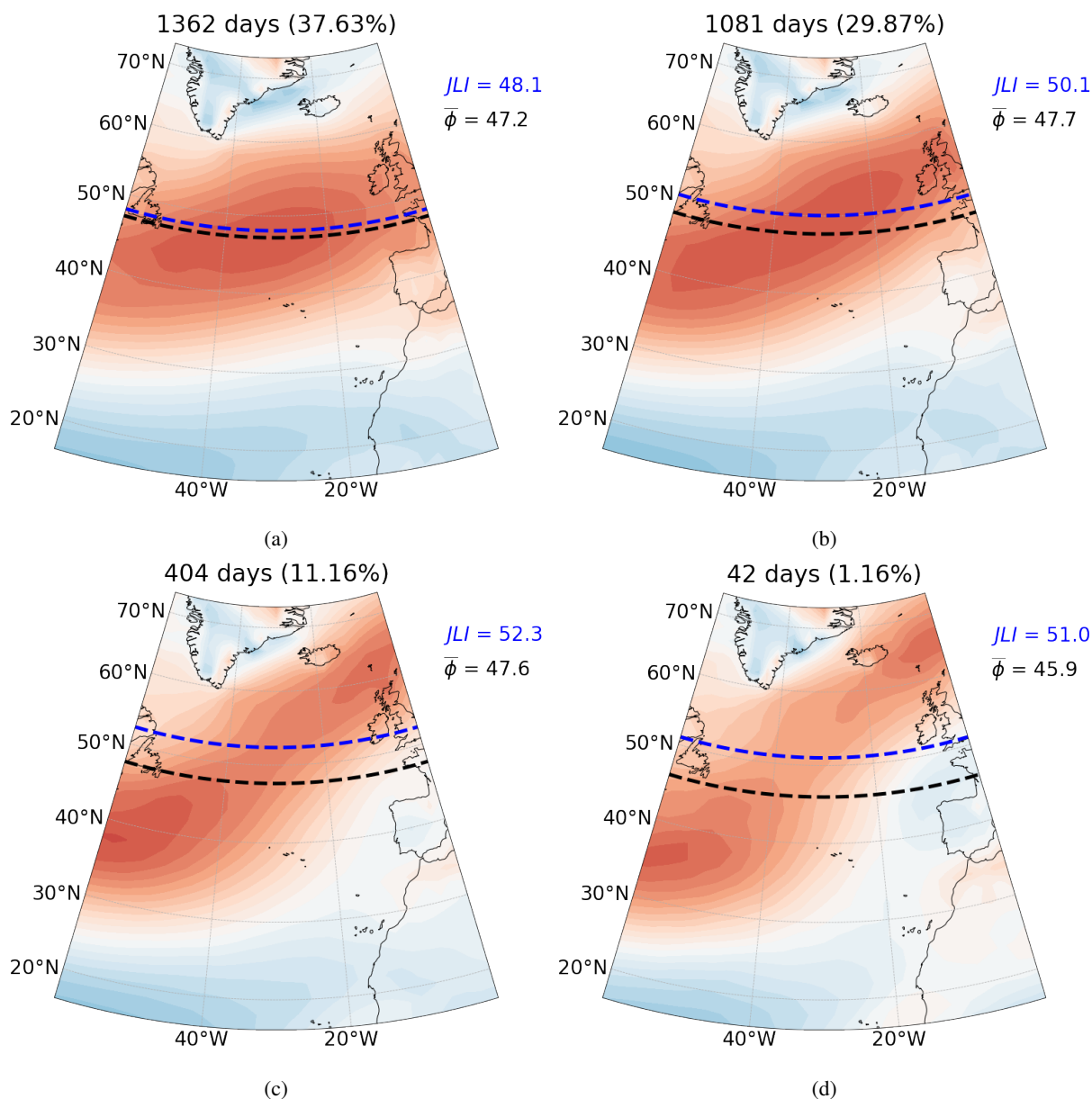
Figure 8. Zonal wind U_{850} composites for positive α where (a) $0 \leq \alpha < 10$, (b) $10 \leq \alpha < 20$, (c) $20 \leq \alpha < 30$ and (d) $\alpha \geq 30$. Dashed lines represent the mean EDJ position for $\overline{\phi}$ (black) and JLI (blue). The number of samples in each composite is given in the header. Similar behaviour is seen for negative α (not shown).

(a)

(b)
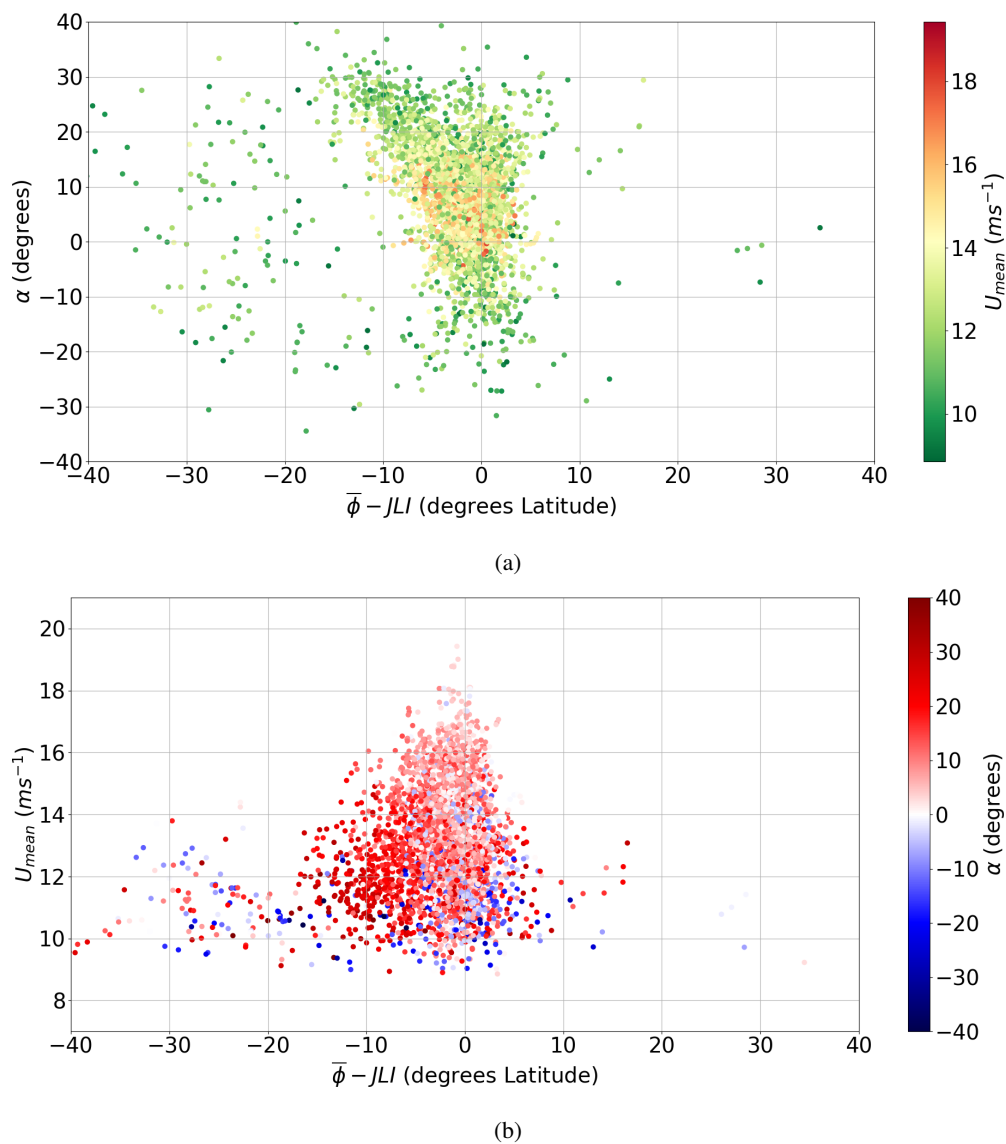
Figure 9. Scatterplots of daily $\overline{\phi} - \mathrm{JLI}$ plotted against α and coloured by U_{mean} in (a) and vice-versa in (b).
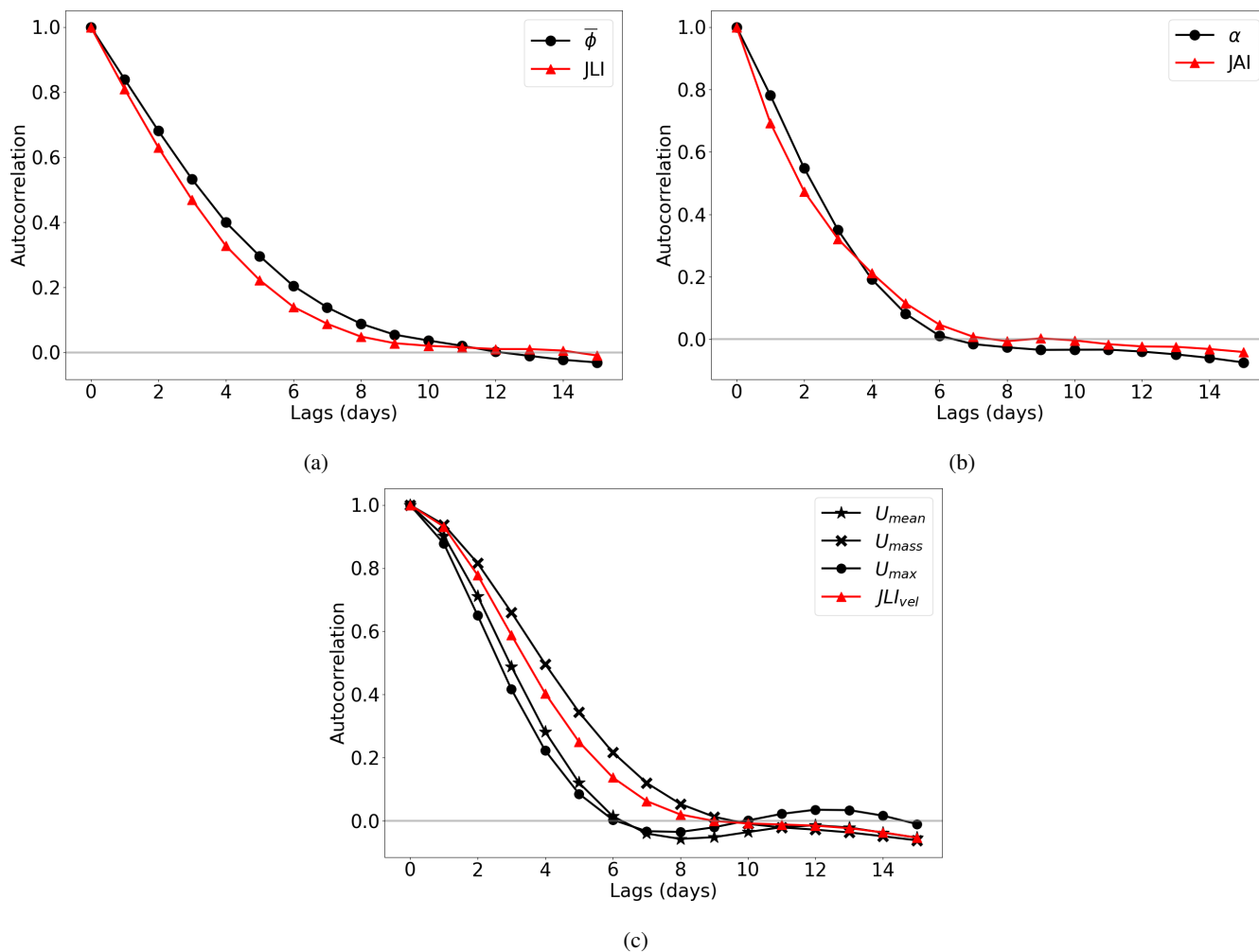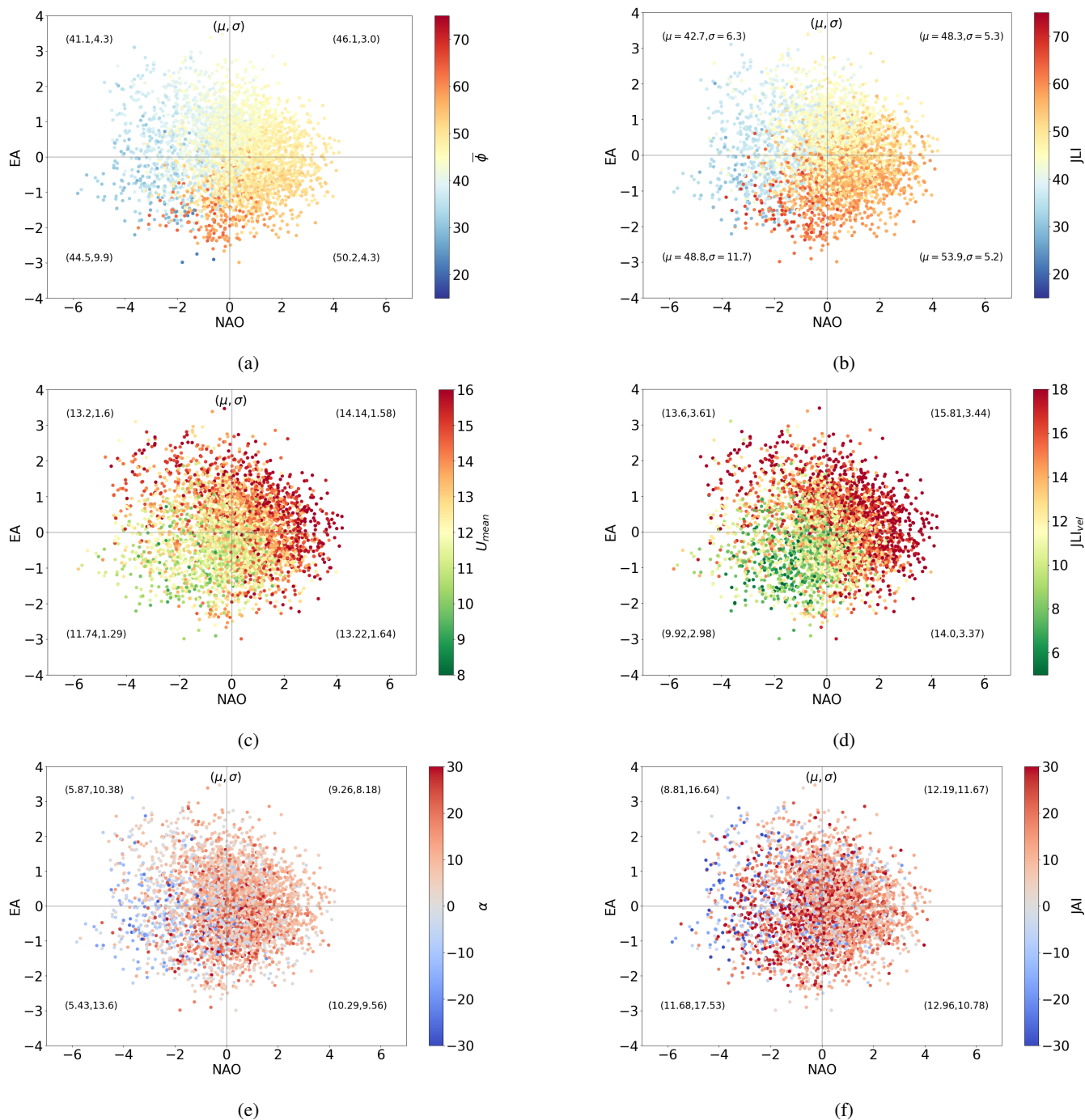
Figure 10. Lagged autocorrelation function for (a) $\overline{\phi}$ (black) and JLI (red), (b) α (black) and JAI (red), and (c) U_{mean}, U_{max}, U_{mass} and JLI$_{vel}$.
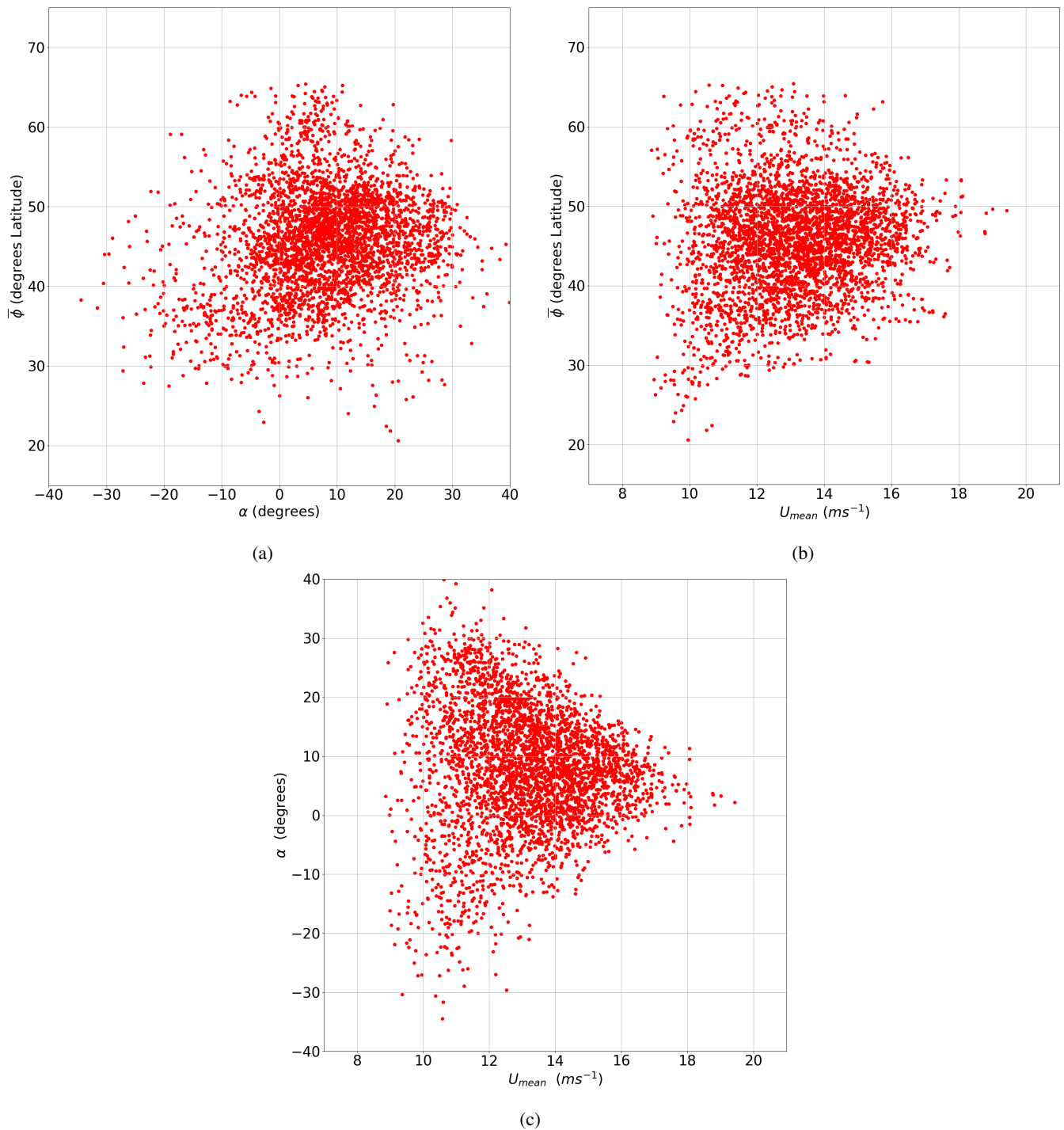
Figure 11. Scatterplots of all winter daily (a) $\overline{\phi}$ vs α, (b) $\overline{\phi}$ vs U_{mean} and (c) α vs U_{mean}.

Figure 12. Scatterplots of all winter daily NAO vs East Atlantic indices coloured by (a) $\overline{\phi}$, (b) JLI, (c) U_{mean}, (d) JLI$_{\mathrm{vel}}$, (e) α and (f) JAI. Note (c) and (d) are shown on different scales and U_{mean} is bounded from below by U_{850}^*. Values of the mean μ and the standard deviation σ for each quadrant is given in brackets.